Journal of Physics: Conference Series

Applications of Vibronic Coupling Density

IOP Conf. Series: Journal of Physics: Conf. Series **1148** (2018) 012004 doi:10.1088/1742-6596/1148/1/012004

Applications of Vibronic Coupling Density

Wataru Ota[1,2] **and Tohru Sato**[*,1,2,3]

[1] Fukui Institute for Fundamental Chemistry, Kyoto University, Sakyo-ku, Kyoto 606-8103, Japan
[2] Department of Molecular Engineering, Graduate School of Engineering, Kyoto University, Nishikyo-ku, Kyoto 615-8510, Japan
[3] Unit of Elements Strategy Initiative for Catalysts & Batteries, Kyoto University, Nishikyo-ku, Kyoto 615-8510, Japan

E-mail: tsato@scl.kyoto-u.ac.jp

Abstract. Vibronic coupling is the interaction between vibrational and electronic motions. The local picture of a vibronic coupling can be expressed in terms of electronic and vibrational structures using vibronic coupling density (VCD). We describe the concepts of vibronic coupling constant (VCC) and VCD within the crude adiabatic approximation, and review their applications to the design of carrier-transporting and light-emitting molecules as well as to the reactivity index for chemical reactions.

1. Introduction

In most quantum chemistry calculations, the Schrödinger equation in which the kinetic energy operator of nuclei is neglected is solved assuming that the masses of the nuclei are heavier than that of an electron. However, the motions of nuclei sometimes play some important roles, as we describe in this review. An adiabatic approximation is usually employed to solve the Schrödinger equation including the nuclear kinetic energy operator. As a result of the adiabatic approximation, a molecular wavefunction, or a vibronic wavefunction, is represented as the product of electronic and vibrational wavefunctions [1–3]. In the crude adiabatic approximation, a vibronic wavefunction is expanded using electronic wavefunctions for a certain nuclear configuration. Thus, the dependencies of nuclear configurations are described only by nuclear wavefunctions. On the other hand, in the Born–Oppenheimer approximation, a vibronic wavefunction is expanded so that both electronic and vibrational wavefunctions depend on nuclear configurations.

We have investigated vibronic coupling, the interaction between vibrational and electronic motions, within the crude adiabatic approximation [4, 5]. Vibronic coupling is quantified by a vibronic coupling constant (VCC). Vibronic coupling density (VCD) is a density form of the VCC. Using the VCD, we can discuss the reason for the small or large values of VCC based on the electronic and vibrational structures. Moreover, VCD analysis enables us to control the VCC by a chemical modification.

A well-known phenomenon induced by vibronic coupling is the Jahn–Teller (JT) effect, in which vibronic coupling lowers the geometrical symmetry of a non-linear molecule with a degenerate electronic state to stabilize the system by a symmetry-lowering deformation to lift the degeneracy of the electronic state [6–8]. The VCC and VCD have been evaluated for JT

systems such as cyclopentadienyl [9, 10], benzene [11], and fullerene [12, 13]. In these studies, the JT vibrational modes that strongly couples to the degenerate electronic states are identified. Various phenomena are related to vibronic coupling other than the JT effect. The applicability of VCD has been extended to non-JT molecules starting from the calculations of naphthalene [14].

In this review article, our recent study on the relations of vibronic coupling to carrier transport, luminescence, and chemical reactions are reviewed. We describe the concepts of VCC and VCD within the crude adiabatic approximation in Sec. 2. Then, we review their applications to the design of carrier-transporting molecules in Sec. 3.1 and light-emitting molecules in Sec. 3.2, and the reactivity index of chemical reactions in Sec. 3.3. In addition, we briefly discuss the perspective towards the applications of VCC and VCD to a solid surface in Sec. 4. Finally, we present conclusions in Sec. 5.

2. Vibronic coupling constant and vibronic coupling density

A Hamiltonian of a molecule with a nuclear configuration $\mathbf{R}$ and electronic coordinates $\mathbf{r}$ is given by

$$\mathcal{H}(\mathbf{r},\mathbf{R}) = \mathcal{H}_e(\mathbf{r},\mathbf{R}) + \mathcal{T}_n(\mathbf{R}). \tag{1}$$

Here, $\mathcal{T}_n(\mathbf{R})$ is a kinetic energy operator of nuclei, and $\mathcal{H}_e(\mathbf{r},\mathbf{R})$ is an electronic Hamiltonian, which is the sum of a kinetic energy operator of electrons, electron-nucleus potential, electron-electron potential, and nucleus-nucleus potential. Using the Herzberg-Teller expansion, $\mathcal{H}_e(\mathbf{r},\mathbf{R})$ is expanded in terms of a normal vibrational coordinate Q_α around an equilibrium reference nuclear configuration $\mathbf{R}_0$ [1, 2]:

$$\mathcal{H}_e(\mathbf{r},\mathbf{R}) = \mathcal{H}_e(\mathbf{r},\mathbf{R}_0) + \sum_\alpha \mathcal{V}_\alpha Q_\alpha + \cdots, \tag{2}$$

where the electronic part of a linear vibronic coupling operator is defined by

$$\mathcal{V}_\alpha = \left(\frac{\partial \mathcal{H}_e(\mathbf{r},\mathbf{R})}{\partial Q_\alpha}\right)_{\mathbf{R}_0}. \tag{3}$$

The quadratic or higher terms are omitted for simplicity. In the crude adiabatic approximation, the vibronic wavefunction, the eigenfunction of the molecular Hamiltonian, with an electronic state i and a vibrational state im is expressed as the product of vibrational wavefunction $|\chi_{im}(\mathbf{Q})\rangle$ and electronic wavefunction $|\Psi_i(\mathbf{x},\mathbf{R}_0)\rangle$:

$$|\Phi_{im}(\mathbf{x},\mathbf{Q})\rangle = |\chi_{im}(\mathbf{Q})\rangle\,|\Psi_i(\mathbf{x},\mathbf{R}_0)\rangle\,, \tag{4}$$

where $\mathbf{x}$ is both the space $\mathbf{r}$ and spin $\boldsymbol{\omega}$ coordinates of the electrons, and $\mathbf{Q}$ is a normal vibrational coordinate. It should be noted that the electronic wavefunction is fixed at $\mathbf{R}_0$. In the Born–Oppenheimer approximation, $|\Phi_{im}(\mathbf{x},\mathbf{Q})\rangle$ is expressed with an electronic wavefunction $|\Psi_i(\mathbf{x},\mathbf{R})\rangle$ that depends on nuclear configurations. The VCC of normal mode α within the crude adiabatic approximation is defined by

$$V_{ij,\alpha} = \langle\Psi_i(\mathbf{x},\mathbf{R}_0)|\mathcal{V}_\alpha|\Psi_j(\mathbf{x},\mathbf{R}_0)\rangle\,. \tag{5}$$

This is called the diagonal VCC ($V_{i,\alpha} := V_{ii,\alpha}$) when $i = j$ and off-diagonal VCC when $i \neq j$. The VCC can be represented as a sum of atomic VCC (AVCC) that describes the contributions from each atom [15]. Using the Hellmann-Feynman theorem [16, 17], the diagonal VCC is written as

$$V_{i,\alpha} = \left(\frac{\partial E_i(\mathbf{R})}{\partial Q_\alpha}\right)_{\mathbf{R}_0}, \tag{6}$$

where $E_i(\mathbf{R})$ are the eigenvalues of $\mathcal{H}_e(\mathbf{r}, \mathbf{R})$. Therefore, the diagonal VCC is calculated from the gradient of a potential energy surface with respect to the normal coordinate at a fixed nuclear configuration.

The VCD is given by the integrand of the VCC [4, 5]:

$$V_{ij,\alpha} = \int \eta_{ij,\alpha}(\boldsymbol{x})\ d^3\boldsymbol{x}, \tag{7}$$

where $\boldsymbol{x} = (x, y, z)$ is the Cartesian coordinate of a single electron Thus, the VCD as a function of $\boldsymbol{x}$ provides a local picture of VCC. The VCD can be decomposed into contributions from the electronic and vibrational structures. The diagonal VCD ($\eta_{i,\alpha} := \eta_{ii,\alpha}$) is represented as

$$\eta_{i,\alpha}(\boldsymbol{x}) = \Delta\rho_i(\boldsymbol{x}) \times v_\alpha(\boldsymbol{x}). \tag{8}$$

Here, $\Delta\rho_i(\boldsymbol{x})$ is the electron density difference defined by

$$\Delta\rho_i(\boldsymbol{x}) = \rho_i(\boldsymbol{x}) - \rho_0(\boldsymbol{x}), \tag{9}$$

where $\rho_i(\boldsymbol{x})$ and $\rho_0(\boldsymbol{x})$ are the electron densities for $|\Psi_i(\mathbf{x}, \mathbf{R}_0)\rangle$ and the equilibrium reference system, respectively. $|\Psi_i(\mathbf{x}, \mathbf{R}_0)\rangle$ is taken, for example, as an ionized state or excited state. $v_\alpha(\boldsymbol{x})$ is the potential derivative defined by

$$v_\alpha(\boldsymbol{x}) = \left(\frac{\partial u(\boldsymbol{x})}{\partial Q_\alpha}\right)_{\mathbf{R}_0}, \tag{10}$$

where $u(\boldsymbol{x})$ is the attractive electron-nucleus potential acting on a single electron. The off-diagonal VCD is represented as

$$\eta_{ij,\alpha}(\boldsymbol{x}) = \rho_{ij}(\boldsymbol{x}) \times v_\alpha(\boldsymbol{x}). \tag{11}$$

Here, $\rho_{ij}(\boldsymbol{x})$ is the overlap density between $|\Psi_i(\mathbf{x}, \mathbf{R}_0)\rangle$ and $|\Psi_j(\mathbf{x}, \mathbf{R}_0)\rangle$:

$$\begin{aligned} \rho_{ij}(\boldsymbol{x}) &= N \int \Psi_i^*(\mathbf{x}, \mathbf{R}_0)\Psi_j(\mathbf{x}, \mathbf{R}_0)\ d\boldsymbol{\omega}_1 d\mathbf{x}_2 \cdots d\mathbf{x}_N \\ &= \cdots \\ &= N \int \Psi_i^*(\mathbf{x}, \mathbf{R}_0)\Psi_j(\mathbf{x}, \mathbf{R}_0)\ d\mathbf{x}_1 \cdots d\mathbf{x}_{N-1} d\boldsymbol{\omega}_N, \end{aligned} \tag{12}$$

where N is the number of electrons. The third equality holds because the electronic wavefunction is antisymmetric with respect to the interchange of electrons. $\rho_{ij}(\boldsymbol{x})$ is equivalent to the electron density for $|\Psi_i(\mathbf{x}, \mathbf{R}_0)\rangle$ when $i = j$. Thus, in the expression of VCD, the electronic structure is described by $\Delta\rho_i(\boldsymbol{x})$ or $\rho_{ij}(\boldsymbol{x})$, and the vibrational structure is described by $v_\alpha(\boldsymbol{x})$.

3. Applications

3.1. Design of carrier-transporting molecules

When a voltage is applied to an electrode-molecule-electrode system, carriers can be transported across the molecule interacting with nuclear vibrations. Since the vibronic coupling causes heat dissipation, developing a molecule with a small vibronic coupling is important for efficient carrier transport. Although both intramolecular and intermolecular vibronic coupling affects the efficiency, only intramolecular vibronic coupling is considered here.

Carbazole derivatives are highly efficient hole-transporting molecules [18, 19]. The VCC and VCD of carbazole are evaluated to clarify the reason in comparison with that of biphenyl and

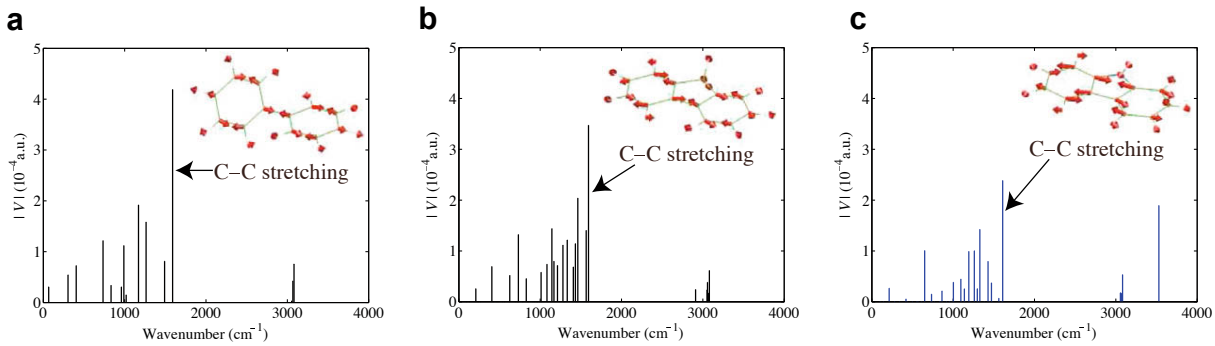

Figure 1. Absolute values of vibronic coupling constants for various cations: (a) biphenyl; (b) fluorene; and (c) carbazole. Reprinted with permission from Ref. [20].

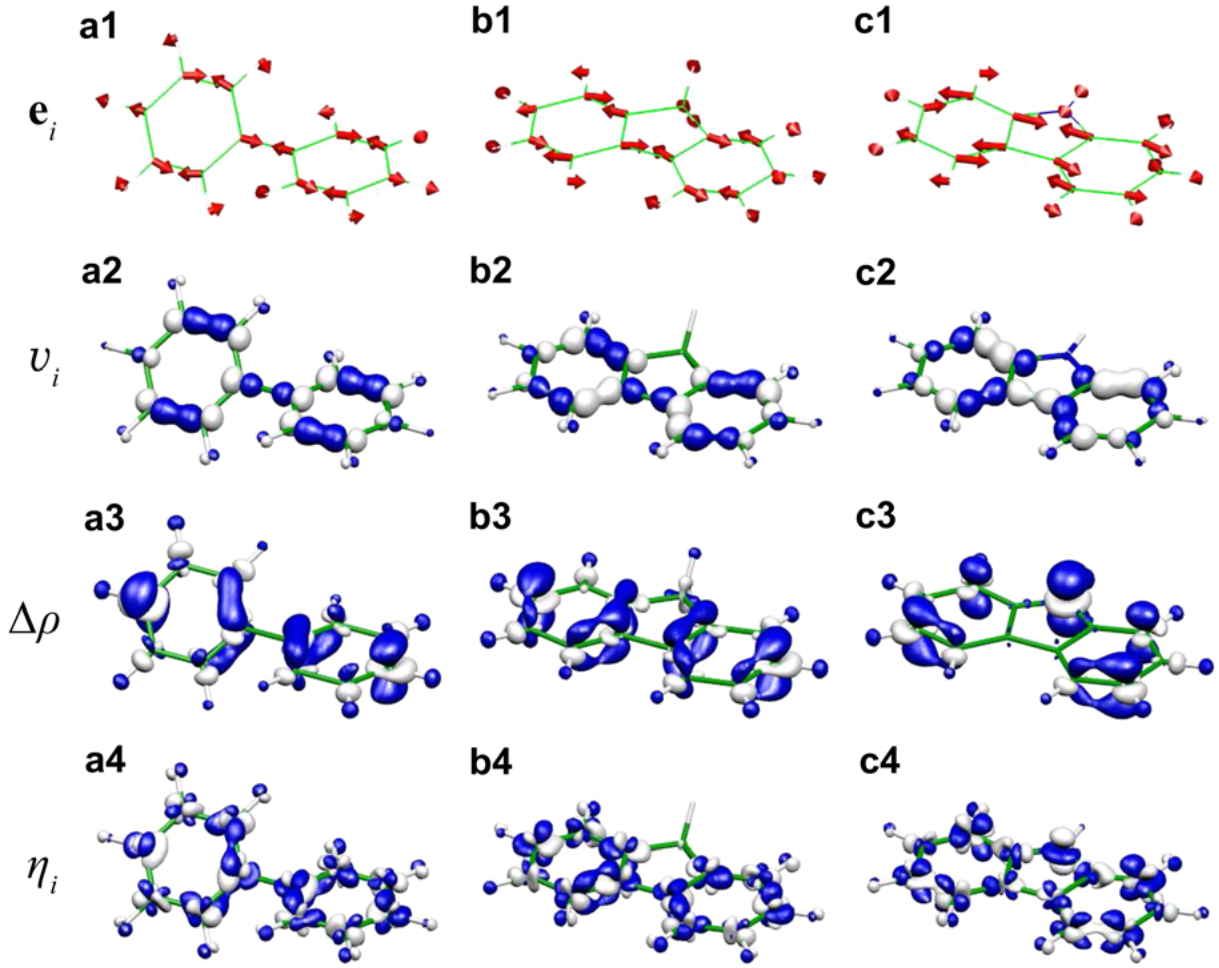

Figure 2. (a1–c1) C-C stretching modes, (a2–c2) corresponding derivatives of the electronic-nuclear potential derivatives v_α, (a3–c3) electron-density differences due to ionization $\Delta\rho_i$, and (a4–c4) vibronic coupling densities of the C-C stretching modes $\eta_{i,\alpha}$: (a1–a4) biphenyl, (b1–b4) fluorene, and (c1–c4) carbazole. White regions are positive; blue regions are negative. Reprinted with permission from Ref. [20].

fluorene having similar structures to that of carbazole [20]. Figure 1 shows the diagonal VCCs of biphenyl, fluorene, and carbazole cations with respect to the strongest coupling modes. In these molecules, the vibrational mode that gives the largest VCC is the C-C stretching mode. The values of the largest VCC are calculated as -4.192×10^{-4} a.u. for biphenyl, -3.440×10^{-4} a.u. for fluorene, and -2.390×10^{-4} a.u. for carbazole. The VCC of carbazole is smaller than that of biphenyl and fluorene, which indicates that intramolecular vibronic coupling is the weakest in carbazole. Figures 2 (a1–c1) and (a2–c2) show the C-C stretching modes and its potential derivatives v_α. Biphenyl, fluorene, and carbazole exhibit similar distributions of v_α that has positive and negative phases symmetrically around the C atoms. Figures 2 (a3–c3) and (a4–c4) show the electron density differences $\Delta\rho_i$ due to cationization and the diagonal VCD $\eta_{i,\alpha}$. $\Delta\rho_i$ is extensively distributed on benzene rings in biphenyl and fluorene, whereas the distribution on benzene rings is relatively suppressed in carbazole. In addition, $\Delta\rho_i$ is localized on the N atom in carbazole where v_α has small values on the N atom. Therefore, $\eta_{i,\alpha}$, which is expressed as the product of v_α and $\Delta\rho_i$, decreases for carbazole, resulting in a small VCC. The localization of $\Delta\rho_i$ on a N atom is also responsible for the weak vibronic coupling in N,N'-diphenyl-N,N'-di(m-tolyl)benzidine (TPD) [21] and triphenylamine (TPA) [15].

Based on the analysis of VCD, hexaboracyclophane [22] and hexaaza[1_6]parabiphenylophane [23] have been proposed as highly efficient carrier-transporting molecules with a weak vibronic coupling.

3.2. Design of light-emitting molecules

Theoretical design of highly efficient light-emitting molecules is of interest for application to organic light-emitting diodes. The important factor for efficiency is the fluorescence quantum yield, which is determined from the ratio of the radiative and nonradiative processes. Therefore, the molecule should be designed such that the radiative process is enhanced, whereas the nonradiative process is suppressed. The nonradiative process includes vibrational relaxation, internal conversion, and intersystem crossing. In this review, the relations of vibronic coupling to vibrational relaxation and internal conversion are described. The radiative process is also discussed because it can be controlled by analysing the transition dipole moment density (TDMD), as the nonradiative process is controlled from the analysis of VCD. Furthermore, the radiative rate constant depends on a Frack-Condon factor, which is calculated using diagonal VCCs.

Assuming that the motions of nuclei are slow compared with that of electrons, a vertical transition occurs from a ground S_0 state to a Franck–Condon state by the absorption of a photon. A molecule at the Franck–Condon state transforms into an adiabatic state through vibrational relaxation. The molecule is stabilized due to vibrational relaxation by dissipating the vibrational energy to the surrounding environment. Within the crude adiabatic approximation, the potential energy surface at the S_i state is represented as [24]

$$E_i(\mathbf{R}) = E_i(\mathbf{R}_0) + \sum_\alpha \left\{ \frac{\omega_{i,\alpha}^2}{2} \left(Q_\alpha - \frac{V_{i,\alpha}}{\omega_{i,\alpha}^2} \right)^2 - \frac{V_{i,\alpha}^2}{2\omega_{i,\alpha}^2} \right\}, \tag{13}$$

where $\omega_{i,\alpha}$ is the frequency of vibrational mode α. The minima of the energy surface for each vibrational mode are stabilized by $-V_{i,\alpha}^2/2\omega_{i,\alpha}^2$ with the shift of $V_{i,\alpha}/\omega_{i,\alpha}^2$ in the direction of Q_α. The total stabilization energy due to the vibrational relaxation is estimated as

$$\Delta E_i = \sum_\alpha \frac{V_{i,\alpha}^2}{2\omega_{i,\alpha}^2}. \tag{14}$$

Thus, the vibrational relaxation can be reduced by decreasing the values of diagonal VCC. It should be noted that the Duschinsky effect is neglected in Eq. (14). In other words, the

normal modes in an excited state is assumed to be the same as that in a ground state. The Duschinsky effect on the stabilization energy is evaluated from the quadratic VCC [24]. Within the Born–Oppenheimer approximation, the stabilization energy including the Duschinsky effect is calculated from the difference in the energies of the Franck–Condon S_i state and S_i state at an equilibrium nuclear configuration.

Since vibrational relaxation is a rapid process, radiative transition and internal conversion mostly occur at the adiabatic state. Assuming that the internal conversion occurs from $|\Phi_{im}\rangle = |\chi_{im}\rangle |\Psi_i\rangle$ to $|\Phi_{jn}\rangle = |\chi_{jn}\rangle |\Psi_j\rangle$, the rate constant of internal conversion from S_i to S_j states is given by [24]

$$k_{i\to j}^{\mathrm{IC}}(T) = \frac{2\pi}{\hbar} \sum_{\alpha} |V_{ij,\alpha}|^2 \sum_{mn} P_{im}(T) \langle \chi_{jn}|Q_\alpha|\chi_{im}\rangle^2 \, \delta(E_{jn} - E_{im}), \tag{15}$$

where $P_{im}(T)$ is the Boltzmann distribution at $|\Phi_{im}\rangle$ with temperature T, and E_{im} and E_{jn} are the eigenvalues corresponding to $|\Phi_{im}\rangle$ and $|\Phi_{jn}\rangle$, respectively. In Eq. (15), the term involving two vibrational modes is neglected. Thus, the internal conversion can be suppressed by decreasing the values of off-diagonal VCC. $k_{i\to j}^{\mathrm{IC}}$ also depends on the diagonal VCC through $\langle \chi_{jn}|Q_\alpha|\chi_{im}\rangle$. Neglecting the Duschinsky effect, the initial vibrational state $|\chi_{im}\rangle$ is expressed as a product of the independent initial states $|n_{i,\alpha}\rangle$ with the number of phonons $n_{i,\alpha}$. Similarly, the final vibrational state $|\chi_{jn}\rangle$ is expressed as a product of the independent final states $|n'_{j,\alpha}\rangle$ with the number of phonons $n'_{j,\alpha}$. As a result,

$$\langle \chi_{jn}|Q_\alpha|\chi_{im}\rangle = \langle n'_{j,\alpha}|Q_\alpha|n_{i,\alpha}\rangle \prod_{\beta\neq\alpha} \langle n'_{j,\beta}|n_{i,\beta}\rangle \tag{16}$$

with [25]

$$\langle n'_{j,\alpha}|n_{i,\alpha}\rangle = \sqrt{\frac{n_{i,\alpha}! n'_{j,\alpha}!}{2^{n_{i,\alpha}+n'_{j,\alpha}}}} e^{-\frac{1}{4}g_{i,\alpha}^2} \sum_{l=0}^{\min[n_{i,\alpha},n'_{j,\alpha}]} (-1)^{n'_{j,\alpha}-l} 2^l \frac{g_{i,\alpha}^{n_{i,\alpha}+n'_{j,\alpha}-2l}}{l!(n_{i,\alpha}-l)!(n'_{j,\alpha}-l)!}, \tag{17}$$

where $g_{i,\alpha} = V_{i,\alpha}/\sqrt{\hbar\omega_{i,\alpha}^3}$ is the dimensionless VCC. Eq. (15) is based on the crude adiabatic approximation. The rate constant of internal conversion based on the Born–Oppenheimer approximation has been derived in Refs. [26–28].

The rate constant of radiative transition from S_i to S_j states is given by [24]

$$k_{i\to j}^{\mathrm{r}}(T) = \int_0^\infty d\omega \frac{4\omega^3}{3c^3} \sum_{mn} P_{im}(T) |\mu_{ij}|^2 \langle \chi_{im}|\chi_{jn}\rangle^2 \, \delta(\hbar\omega - E_{im} + E_{jn}), \tag{18}$$

where ω and c are the angular frequency and speed of photon, respectively. μ_{ij} is the transition dipole moment between $|\Psi_i\rangle$ and $|\Psi_j\rangle$, which affects the enhancement of radiative transition rate. The VCD is introduced as the integrand of VCC to control its value based on the local picture. In a similar manner, the TDMD is introduced as the integrand of transition dipole moment [5]:

$$\mu_{ij} = \int \tau_{ij}(\boldsymbol{x}) \, d^3\boldsymbol{x}. \tag{19}$$

τ_{ij} is represented using the overlap density between S_i and S_j states as

$$\tau_{ij}(\boldsymbol{x}) = -e\boldsymbol{x}\rho_{ij}(\boldsymbol{x}), \tag{20}$$

where e is the charge of an electron.

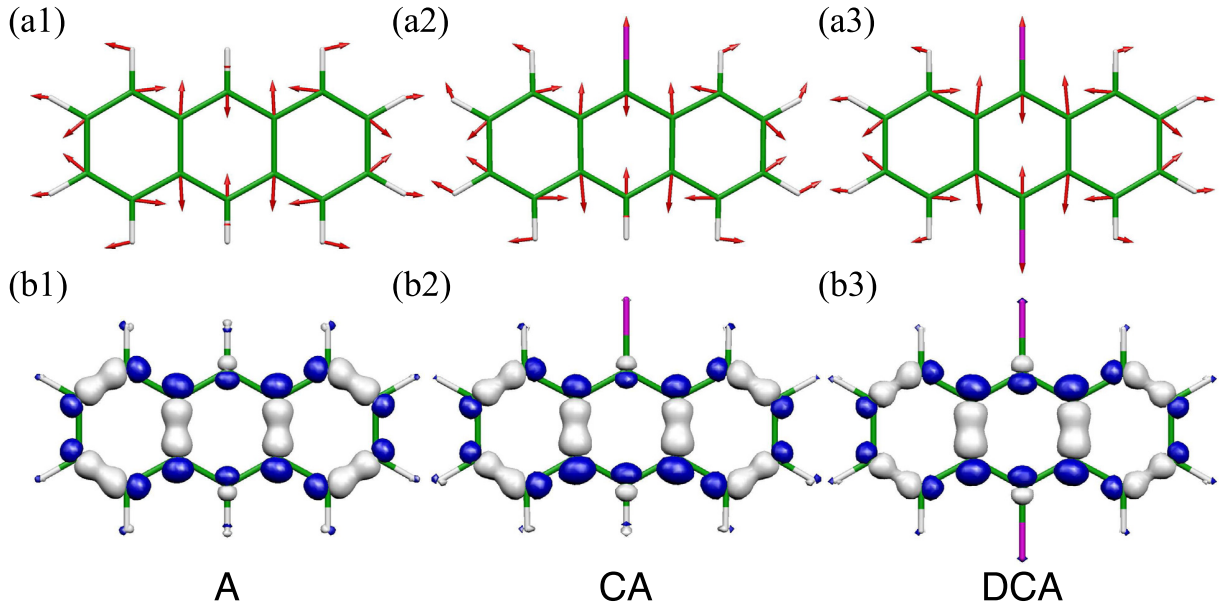

Figure 3. (a1–a3) Vibrational modes susceptible to chlorinations and (b1–b3) derivatives of electronic-nuclear potentials with respect to their modes v_α: (a1, b1) **A** ($\omega_{48} = 1427.55$ cm^{-1}), (a2, b2) **CA** ($\omega_{48} = 1420.09$ cm^{-1}), and (a3, b3) **DCA** ($\omega_{49} = 1409.13$ cm^{-1}). White regions are positive; blue regions are negative. Reprinted with permission from Ref. [29].

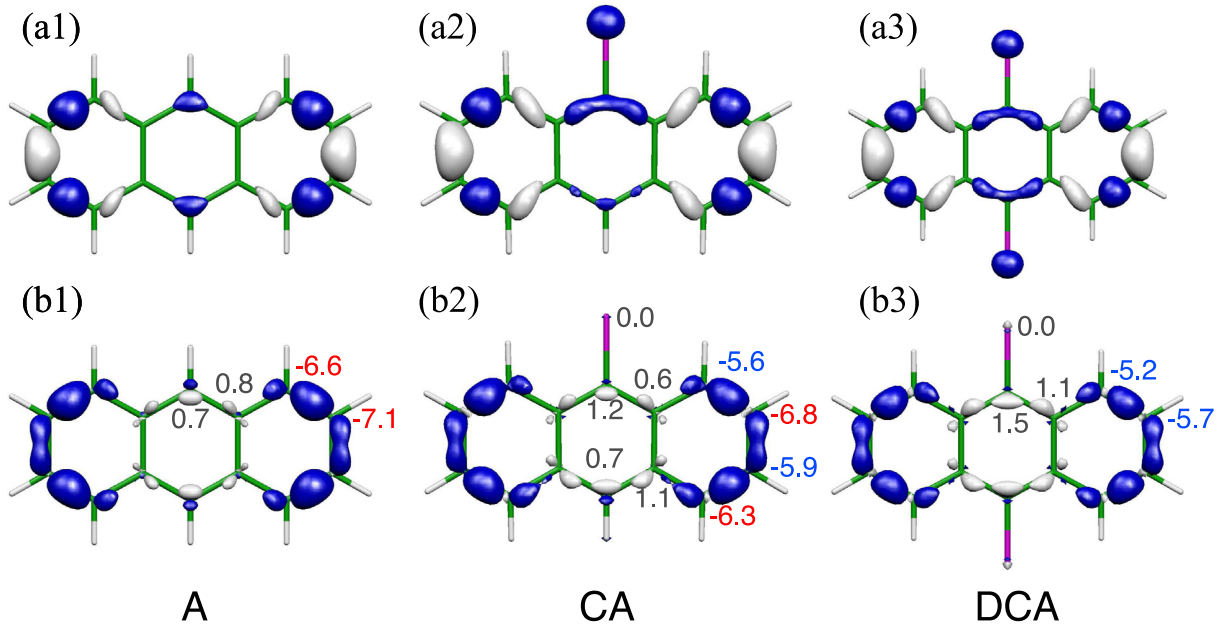

Figure 4. (a1–a3) Electron-density differences between S_1 and S_0 states $\Delta\rho_1$ and (b1–b3) diagonal vibronic coupling densities in the Franck–Condon S_1 state for normal modes susceptible to chlorinations $\eta_{1,\alpha}$: (a1,b1) **A**, (a2,b2) **CA**, and (a3,b3) **DCA**. Atomic vibronic coupling constants in 10^{-5} a.u. are shown in (b1–b3). Large AVCC values are shown in red and those reduced significantly by chlorinations are shown in blue. White regions are positive; blue regions are negative. Reprinted with permission from Ref. [29].

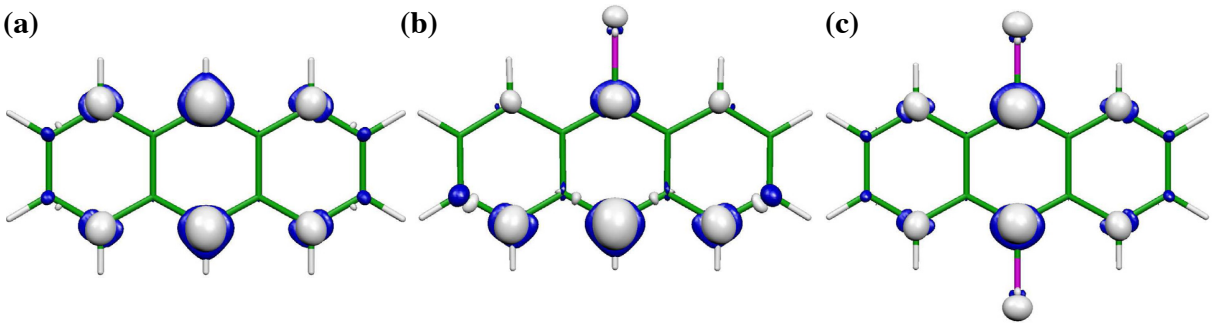

Figure 5. Transition dipole moment densities between S_1 and S_0 states in z direction $\tau_{10,z}$, for (a) **A**, (b) **CA**, and (c) **DCA**. White regions are positive; blue regions are negative. Reprinted with permission from Ref. [29].

A design principle for fluorescent anthracene derivatives, which are candidates for highly efficient emitting molecules in an organic light-emitting diode (OLED), has been proposed from the analyses of VCD and TDMD [29, 30]. The fluorescence quantum yields of anthracene (**A**), 9-chloroanthracene (**CA**), and 9,10-chloroanthracene (**DCA**) were experimentally evaluated as 0.33, 0.11, and 0.53, respectively [31]. First, the contribution of vibrational relaxation to the quantum yield is discussed [29]. Figure 3 shows the vibrational modes of **A**, **CA**, and **DCA** susceptible to chlorinations, and the potential derivatives v_α with respect to the susceptible modes. The modes and v_α exhibit similar behaviours regardless of chlorinations. Figire 4 shows the electron density differences $\Delta\rho_1$ between S_1 and S_0 states, and the diagonal VCD $\eta_{1,\alpha}$. $\Delta\rho_1$ are large at the C atoms bonded to the Cl atoms in **CA** and **DCA**. As a result, $\eta_{1,\alpha}$, the product of v_α and $\Delta\rho_1$, has large positive values on these C atoms although $\eta_{1,\alpha}$ localized on the edges of **CA** and **DCA** are negative. Therefore, the diagonal VCCs obtained by the integration of diagonal VCD are small in **CA** and **DCA** compared to **A**, which explains the order of the calculated stabilization energies: 0.2332 eV for **A**, 0.2275 eV for **CA**, and 0.2211 eV for **DCA**. Although the vibrational relaxation is suppressed in **CA** and **DCA**, the quantum yield of **CA** is lower than that of **A**. This is attributed to the difference in the internal conversion rate. The square sums of off-diagonal VCC, $\sum_\alpha |V_{10,\alpha}|$, are calculated as 1.30×10^{-4} a.u. for **A**, 1.69×10^{-4} a.u. for **CA**, and 1.24×10^{-4} a.u. for **DCA**. According to the selection rule, active vibrational modes that give non-zero VCC are few in a molecule with high symmetry. Therefore, **A** and **DCA** with D_{2h} symmetry have a smaller number of active modes than **CA** with C_{2v} symmetry does, which results in the suppression of internal conversion in **A** and **DCA**. Finally, the TDMD is shown in Figure 5 to evaluate the radiative transition rate. The TDMD is large on Cl atoms because the overlap density ρ_{10} is localized on the Cl atoms. Therefore, the transition dipole moment is increased in **CA** and, even more, in **DCA**. Indeed, the oscillator strengths, proportional to the square of the transition dipole moment, are large in the order of 0.0542 for **A**, 0.0700 for **CA**, and 0.0899 for **DCA**. Since the TDMD is the product of ρ_{10} and distance from the origin, the localization of ρ_{10} away from the origin leads to the enhancement of radiative transition. Consequently, the design principle is summarized as follows: long substituents on which the overlap density is localized should be introduced, and the D_{2h} symmetry should be maintained. Following these design principles, an anthracene derivative, 5,11-bis(phenylethynyl)benzo[1,2-f:4,5-f′]diisoindole-1,3,7,9(2*H*,8*H*)-tetraone, was designed and synthesized [30]. The observed fluorescence quantum yield of the rationally designed molecule was 96 %.

In addition to the anthracene derivatives, a design principle for triphenylamine derivatives was presented [32]. Furthermore, a novel electroluminescence mechanism in OLEDs utilizing higher

triplet states than the T_1 state, called fluorescence via higher triplets (FvHT) mechanism, has been proposed based on the analyses of VCD and TDMD [33–35].

3.3. Reactivity index for chemical reactions

One of the important problems in quantum chemistry is the specification of reactive sites in a molecule. In the early stage of chemical reactions, a reacting system is stabilized by the charge transfer between the reactants. The stabilization arising from the charge-transfer interactions are evaluated from the frontier orbital theory [36–38]. After the charge transfer, the reacting system is further stabilized through a structural relaxation caused by vibronic couplings. The frontier orbital theory has been successfully used for explaining the regioselectivity of chemical reactions. However, it does not consider the effect of vibronic couplings on the stabilization, which sometimes leads to the failure of the prediction of regioselectivity.

Parr and Yang rationalized the frontier orbital theory of chemical reactivity based on the conceptual density functional theory [39–41]. The chemical potential $\mu[N, u]$, which is a functional of the number of electrons N and the attractive electron-nucleus potential u, is given by

$$d\mu = 2\eta_N dN + \int f(\boldsymbol{x})\ du d^3\boldsymbol{x}, \tag{21}$$

where $\eta_N = 1/2(\partial\mu/\partial N)_u$ is the absolute hardness, and $f(\boldsymbol{x}) = [\delta\mu/\delta u(\boldsymbol{x})]_N$ is the Fukui function. The reagent attacks a site to maximize the change in chemical potential $|d\mu|$, particularly a site where $f(\boldsymbol{x})$ is the largest. Thus, $f(\boldsymbol{x})$ as a function of $\boldsymbol{x}$ is regarded as a reactivity index of chemical reactions. The Fukui function is approximated to the highest occupied molecular orbital (HOMO) density for electrophilic reactions and the lowest unoccupied molecular orbital (LUMO) density for nucleophilic reactions.

Assuming that the Fukui function is replaced with the electron density difference between the charge-transfer state and the reference state, the total differential of chemical potential is given by [14, 42]

$$d\mu = 2\eta_N dN + \int \eta_s(\boldsymbol{x})\ ds d^3\boldsymbol{x}, \tag{22}$$

where $\eta_s(\boldsymbol{x})$ is the VCD of reaction mode s along which the chemical reaction occurs. $\eta_s(\boldsymbol{x})$ is represented as the product of electron density difference due to charge transfer and potential derivative in terms of s. The corresponding VCC is obtained from the gradient of the potential energy surface in the charge-transfer state with respect to s, as expressed in Eq. (6). The reaction mode is taken as an effective mode defined by

$$ds = \sum_\alpha \frac{V_\alpha}{\sqrt{\sum_\alpha V_\alpha^2}}\ dQ_\alpha, \tag{23}$$

which coincides with the steepest descent direction to the minimum of the potential energy surface in the charge-transfer state. Thus, according to the principle proposed by Parr and Yang, the VCD can be regarded as a reactivity index that maximizes $|d\mu|$. It should be noted that $\eta_s(\boldsymbol{x})$, in contrast to $f(\boldsymbol{x})$, includes the effects of not only electronic but also vibrational structures on chemical reactivity. The VCD can be extended in the finite-temperature grand-canonical ensemble, which can be applied for charge transfer involving a fractional number of electrons [43].

The VCD as a reactivity index is applied to investigate the regioselectivity of cycloaddition reactions of fullerene [42, 44–46], matallofullerene [47], and polycyclic aromatic hydrocarbons [48]. The frontier orbital theory has difficulty in predicting the regioselectivity of these reactions because the frontier orbitals tend to delocalize in such large systems. C_{60} fullerene undergoes nucleophilic cycloaddition reactions at the 6,6-bonds between two hexagonal rings rather than

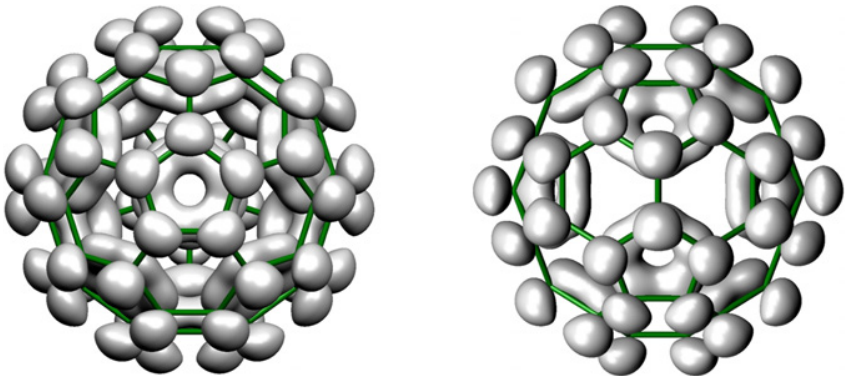

Figure 6. Averaged density of LUMOs. Reprinted with permission from Ref. [42].

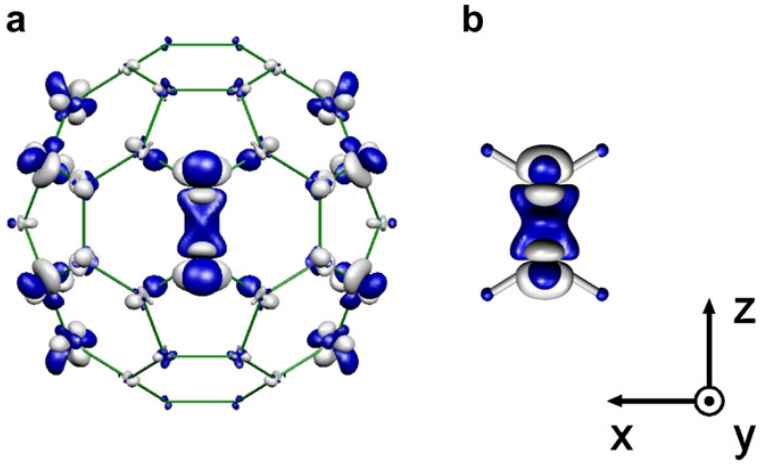

Figure 7. Vibronic coupling density analysis for the reaction mode in (a) C_{60}^{-} and (b) ethylene monoanion. Reprinted with permission from Ref. [42].

the 6,5-bonds between the hexagonal and pentagonal rings [49, 50]. Figure 6 shows the LUMO density of C_{60} [42]. Since the LUMO density is delocalized in the entire molecule, the reactive sites in C_{60} cannot be identified by the frontier orbital theory. In contrast, Figure 7 shows the VCD of C_{60}^{-} with respect to the effective mode, which is strongly localized on the 6,6-bonds. Therefore, the VCD clearly elucidates the reactive sites of C_{60}. In addition, the VCD of C_{60}^{-} is analogous to that of ethylene monoanion, which implies that C_{60} undergoes nucleophilic reactions in a similar manner to ethylene. The reactive sites for multiple cycloadditions to C_{60} are obtained in agreement with experiments by successively calculating the VCD of C_{60} adducts [45, 46].

4. Perspective towards a solid surface

In Sec. 3, the applications of VCC and VCD concepts to molecules are discussed. Vibronic coupling also influences phenomena in a solid surface such as a heterogeneous catalyst. Vanadium oxide highly dispersed on silica is a photocatalyst that oxidises light alkanes and alkenes [51–53]. The active centre reacting with these compounds is experimentally observed to be a terminal oxygen in the isolated VO_4 at the T_1 state [54]. It is predicted that the appearance of an active centre is because of the JT effect [55, 56]. The isolated VO_4 on silica is modelled such that three basal O atoms are bonded to H atoms instead of silica. Figure 8 shows the frontier orbitals of

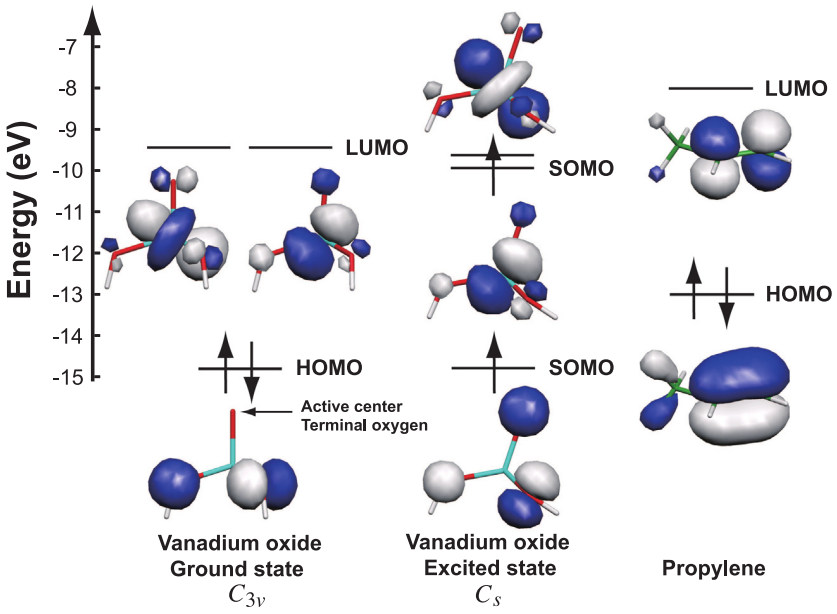

Figure 8. Frontier orbitals of the active species. HOMO and LUMO with C_{3v} are shown on the left, those with Jahn–Teller distortion are shown in the middle, and HOMO and LUMO of propylene are shown on the right. Reprinted with permission from Ref. [56].

H_3VO_4 and propylene as an example of oxidised alkene [56]. The HOMO of H_3VO_4 with C_{3v} symmetry has no molecular orbital coefficients on the terminal oxygen. However, the doubly degenerate LUMOs cause JT distortion to the C_s symmetry in the T_1 state. As a result, the low-lying singly occupied molecular orbital (SOMO) has coefficients on the terminal oxygen. This is because the doubly degenerate next HOMOs, which have coefficients on the terminal oxygen in the C_{3v} symmetry, interact with the HOMO along with the JT distortion. Thus, the JT distortion results in the appearance of an active centre in the SOMO.

In the above calculations, the effect of silica surface on the catalytic activity in VO_4 is neglected. However, the activity generally varies with the type of catalytic support. The applications of VCC and VCD concepts to a solid surface can shed light on the origin of the activity of heterogeneous catalysts.

5. Conclusion

We reviewed our recent study on the applications of VCC and VCD to a molecule. Vibronic coupling in carrier-transporting and light-emitting molecules can be suppressed by investigating the origin of VCC from VCD analysis, which enables us to design efficient functional molecules by a chemical modification. The VCD can also be used as a reactivity index for large molecules that has difficulty in predicting the regioselectivity due to the delocalization of the frontier orbital. The applications of VCC and VCD to a solid surface is desired for revealing the mechanism of heterogeneous catalysts.

Acknowledgment

This study was supported by Elements Strategy Initiative for Catalysts and Batteries (ESICB), JSPS KAKENHI Grant Number JP18K05261 in Scientific Research (C), and JSPS KAKENHI Grant Number JP17H05259 in Scientific Research on Innovative Areas “Photosynergetics”.

References

[1] Fischer G 1984 *Vibronic Coupling: The Interaction between the Electronic and Nuclear Motions* (London: Academic Press)
[2] Bersuker I B and Polinger V Z 1989 *Vibronic Interactions in Molecules and Crystals* (Berlin: Springer-Verlag)
[3] Azumi T and Matsuzaki K 1977 *Photochem. Photobiol.* **25** 315
[4] Sato T, Tokunaga K, Iwahara N, Shizu K and Tanaka K 2009 Vibronic coupling constant and vibronic coupling density *The Jahn-Teller Effect: Fundamentals and Implications for Physics and Chemistry* ed Köppel H, Yarkony D R and Barentzen H (Berlin and Hidelberg: Springer-Verlag) pp 99–129
[5] Sato T, Uejima M, Iwahara N, Haruta N, Shizu K and Tanaka K 2013 *J. Phys.: Conf. Ser.* **428** 012010
[6] Jahn H A and Teller E 1937 *Proc. R. Soc. A* **161** 220
[7] Bersuker I 1984 *The Jahn-Teller Effect and Vibronic Interactions in Modern Chemistry* (New York: Plenum)
[8] Bersuker I B 2001 *Chem. Rev.* **101** 1067
[9] Sato T, Tokunaga K and Tanaka K 2006 *J. Chem. Phys.* **124** 024314
[10] Tokunaga K, Sato T and Tanaka K 2007 *J. Mol. Struct.* **838** 116
[11] Tokunaga K, Sato T and Tanaka K 2006 *J. Chem. Phys.* **124** 154303
[12] Iwahara N, Sato T, Tanaka K and Chibotaru L F 2010 *Phys. Rev. B* **82** 245409
[13] Iwahara N, Sato T and Tanaka K 2012 *J. Chem. Phys.* **136** 174315
[14] Sato T, Tokunaga K and Tanaka K 2008 *J. Phys. Chem. A* **112** 758
[15] Shizu K, Sato T, Tanaka K and Kaji H 2010 *Chem. Phys. Lett.* **486** 130
[16] Hellmann H 1937 *Einführung in die Quantenchemie* (Leipzog: Deuticke and Company)
[17] Feynman R P 1939 *Phys. Rev.* **56** 340
[18] Koene B E, Loy D E and Thompson M E 1998 *Chem. Mater.* **10** 2235
[19] Zhang Q, Chen J, Cheng Y, Wang L, Ma D, Jing X and Wang F 2004 *J. Mater. Chem.* **14** 895
[20] Shizu K, Sato T, Tanaka K and Kaji H 2010 *Org. Electro.* **11** 1277
[21] Sato T, Shizu K, Kuga T, Tanaka K and Kaji H 2008 *Chem. Phys. Lett.* **458** 152
[22] Shizu K, Sato T, Tanaka K and Kaji H 2010 *Appl. Phys. Lett.* **97** 142111
[23] Shizu K, Sato T, Ito A, Tanaka K and Kaji H 2011 *J. Mater. Chem.* **21** 6375
[24] Uejima M, Sato T, Yokoyama D, Tanaka K and Park J W 2014 *Phys. Chem. Chem. Phys.* **16** 14244
[25] Hutchisson E 1930 *Phys. Rev.* **36** 410
[26] Peng Q, Yi Y, Shuai Z and Shao J 2007 *J. Chem. Phys.* **126** 114302
[27] Peng Q, Yi Y, Shuai Z and Shao J 2007 *J. Am. Chem. Soc.* **129** 9333
[28] Niu Y, Peng Q, Deng C, Gao X and Shuai Z 2010 *J. Phys. Chem. A* **114** 7817
[29] Uejima M, Sato T, Tanaka K and Kaji H 2014 *Chem. Phys.* **430** 47
[30] Uejima M, Sato T, Detani M, Wakamiya A, Suzuki F, Suzuki H, Fukushima T, Tanaka K, Murata Y, Adachi C *et al.* 2014 *Chem. Phys. Lett.* **602** 80
[31] Ateş S and Yildiz A 1983 *J. Chem. Soc., Faraday Trans. 1* **79** 2853
[32] Kameoka Y, Uebe M, Ito A, Sato T and Tanaka K 2014 *Chem. Phys. Lett.* **615** 44
[33] Sato T, Uejima M, Tanaka K, Kaji H and Adachi C 2015 *J. Mater. Chem. C* **3** 870
[34] Sato T 2015 *J. Comput. Chem., Jpn.* **14** 189
[35] Sato T, Hayashi R, Haruta N and Pu Y J 2017 *Sci. Rep.* **7** 4820
[36] Fukui K, Yonezawa T and Shingu H 1952 *J. Chem. Phys.* **20** 722
[37] Fukui K, Yonezawa T, Nagata C and Shingu H 1954 *J. Chem. Phys.* **22** 1433
[38] Fukui K 1982 *Science* **218** 747
[39] Parr R G and Yang W 1984 *J. Am. Chem. Soc.* **106** 4049
[40] Parr R G and Yang W 1994 *Density-Functional Theory of Atoms and Molecules* (New York: Oxford University Press)
[41] Parr R and Yang W 1995 *Annu. Rev. Phys. Chem.* **46** 701
[42] Sato T, Iwahara N, Haruta N and Tanaka K 2012 *Chem. Phys. Lett.* **531** 257
[43] Sato T, Haruta N and Tanaka K 2016 *Chem. Phys. Lett.* **652** 157
[44] Haruta N, Sato T and Tanaka K 2012 *J. Org. Chem.* **77** 9702
[45] Haruta N, Sato T, Iwahara N and Tanaka K 2013 **428** 012003
[46] Haruta N, Sato T and Tanaka K 2014 *Tetrahedron* **70** 3510
[47] Haruta N, Sato T and Tanaka K 2014 *J. Org. Chem.* **80** 141
[48] Haruta N, Sato T and Tanaka K 2015 *Tetrahedron Lett.* **56** 590
[49] Yurovskaya M and Trushkov I 2002 *Russ. Chem. Bull. Int. Ed.* **51** 367
[50] Thilgen C and Diederich F 2006 *Chem. Rev.* **106** 5049
[51] Amano F, Tanaka T and Funabiki T 2004 *Langmuir* **20** 4236
[52] Amano F, Yamaguchi T and Tanaka T 2006 *J. Phys. Chem. B* **110** 281
[53] Amano F and Tanaka T 2006 *Chem. Lett.* **35** 468

[54] Teramura K, Hosokawa T, Ohuchi T, Shishido T and Tanaka T 2008 *Chem. Phys. Lett.* **460** 478
[55] Sato T, Iwahara N, Tokunaga K, Tanaka K and Tanaka T 2009 *Top. Catal.* **52** 808
[56] Iwahara N, Sato T, Tanaka K and Tanaka T 2013 *Chem. Phys. Lett.* **584** 63